Bulk FePt/Fe_3Pt nanocomposite magnets prepared by spark plasma sintering

Chuan-Bing Rong, Vikas Nandwana, Narayan Poudyal, and J. Ping Liu[a)]
Department of Physics, University of Texas at Arlington, Arlington, Texas 76019

Tetsuji Saito
Department of Mechanical Science and Engineering, Chiba Institute of Technology, 2-17-1 Tsudanuma, Narashino, Chiba 275-0016, Japan

Yaqiao Wu and Matthew J. Kramer
Ames Laboratory, Iowa State University, Ames, Iowa 50011 and Department of Physics and Astronomy, Iowa State University, Ames, Iowa 50011

(Presented on 8 January 2007; received 27 October 2006; accepted 7 December 2006; published online 27 April 2007)

FePt/Fe_3Pt bulk nanocomposite magnets have been prepared by the spark plasma sintering of chemically synthesized FePt and Fe_3O_4 nanoparticles under 100 MPa at 400–600 °C. It was found that the phase transition of the FePt compound from the face centered cubic to the $L1_0$ started at 500 °C and was almost completed at 600 °C during the sintering. The activated atomic diffusion during the phase transition led to a significant increase in density. The density about 70% of the theoretical value has been obtained. Grain size of the sintered samples remains nanoscale even after a postannealing at 700 °C. Pressure rather than temperature was more effective in enhancing intergrain exchange coupling compared to temperature. © *2007 American Institute of Physics*. [DOI: 10.1063/1.2710811]

Nanocomposite magnets consisting of a hard magnetic phase with high coercivity and a soft magnetic phase with high magnetization have attracted considerable interest since they could potentially provide a maximum energy product $(BH)_{max}$ in excess of 100 MG Oe for anisotropic[1,2] and 35 MG Oe for isotropic magnets.[2–4] The magnetic behavior of these exchange-coupled nanocomposites is closely related to grain size and nanostructured morphology. Effective exchange coupling can be obtained only if dimensions of the soft-phase component in a nanocomposite magnet are not larger than a critical length (typically in the range from several to several tens of nanometers).[5–8] Unfortunately, grain sizes of nanocomposite magnets fabricated by conventional top-down methods are usually much larger than the critical length. Recently, exchange-coupled FePt/Fe_3Pt nanocomposite magnets prepared from chemically synthesized nanoparticles have attracted great interest due to the controllable microstructure and the excellent magnetic properties.[9] However, fabrication of bulk nanocomposite magnets from nanoparticles remains a great challenge. Spark plasma sintering (SPS) is known as one of the sintering and condensation techniques.[10–12] The SPS process utilizes a high-frequency, momentary local heating to obtain compacted and sintered specimen. The high sintering speed can effectively restrain grain growth and allow the formation of high-density fine crystalline materials in a short consolidating time. In this work, we report the structure and magnetic properties of bulk FePt/Fe_3Pt nanocomposite magnets prepared by SPS processing of chemically synthesized FePt and Fe_3O_4 nanoparticles.

The 4 nm disordered face-centered-cubic (fcc) FePt and 6 nm Fe_3O_4 nanoparticles were chemically synthesized by the standard airless chemical solution procedures[13,14] and then were mixed with the mass ratio of about 8:1 in a solution before centrifugation. The dried nanoparticles were heated under Ar atmosphere at 350 °C for 1 h to remove the surfactants. The prepared powders were then placed in a carbon die and sintered under a vacuum by spark plasma sintering at 400, 500, and 600 °C for 600 s. The samples were named as SPS400, SPS500, and SPS600, respectively. A pressure of 100 MPa was applied during the heating of the specimens. The Archimedes method was employed to measure the bulk sample density. The morphology and crystalline structure were characterized by scanning electron microscopy (SEM), transmission electron microscopy (TEM), and x-ray diffraction (XRD) using Cu $K\alpha$ radiation. The chemical ordering parameter S is calculated by the equation $S \cong 0.85[I_{001}/I_{002}]^{1/2}$, where I_{001} and I_{002} are the integrated intensity of (001) and (002) diffraction peaks from XRD patterns, respectively.[15] The composition of the sintered samples was checked by energy dispersive x-ray (EDX) analysis in both SEM and TEM. Magnetic properties were measured with a superconducting quantum interference device (SQUID) magnetometer with a maximum applied field of 70 kOe.

Table I gives the dependence of the compacted density on the sintering temperature T_s. It can be seen that the density increased with increasing T_s which can be attributed to the monotonic decrease of yield strength of the FePt phase with temperature.[16] When $T_s > 500$ °C, it is interesting to find that the compacted density increased nonlinearly with T_s. It cannot be simply explained with the yield strength-

[a)]Electronic mail: pliu@uta.edu

TABLE I. The dependence of the compact density and oxygen percent on T_s.

T_s	Compacted density (g/cm^3)	Relative density (%)	Oxygen percent (%)
RT	6.2±0.2	42.8±1.5	12.4±0.7
400 °C	7.5±0.3	51.7±2.1	10.5±0.6
500 °C	7.8±0.2	53.8±1.5	7.8±0.8
600 °C	10.1±0.4	70.0±2.5	2.5±0.9

temperature relationship and may be related to the phase transition of FePt phase from disordered fcc to ordered $L1_0$ structure during the sintering, which will be discussed in detail later. As we know, the atoms are activated during the phase transition and are more mobile than the situation without a phase transition since they need to rearrange themselves during the phase transformation. The enhanced atomic diffusion promoted densification of the compacts and resulted in a high density. Similar phenomenon has also been observed in our warm compaction experiments. Figure 1 shows the typical SEM images of the sintered samples. The SPS400 sample is mainly consisted of small particles (around 1 μm) while some large particles are formed. With increasing T_s to 500 °C, the particle size increased slightly. Sintering at 600 °C led to the significant growth of particles (around 50 μm) and thus the highest density. As a result, the SPS600 has the highest density (about 10.1 g/cm^3) which is 70% of the theoretical value. This value is far lower than the density that can be achieved by the SPS technique for micro-sized particles.[10–12]

Shown in Fig. 2 are the XRD patterns of the starting powders and the sintered bulk samples. The SPS400 contains fcc FePt and Fe_3O_4. Phase transition from fcc to $L1_0$ took place at 500 °C, while most of the Fe_3O_4 phase is retained. By 600 °C sintering, $L1_0$ FePt was fully developed and Fe_3O_4 phase almost disappeared. Fe_3Pt may be formed during the phase transition.[9] Approximately 13% volume fraction of Fe_3Pt phase in SPS600 was determined by using the method Rietveld refinement of the XRD pattern.[17,18] EDX analysis shows that the oxygen percent decreases from 10.5% for SPS400 to 2.5% for SPS600, which agrees with the XRD results showing the disappearance of Fe_3O_4 and formation of Fe_3Pt. The Fe_3O_4 decomposition temperature is much lower than that reported in the literature.[19] This may be attributed to the vacuum condition during the sintering or the activated atom diffusion during the phase transition of FePt component.

Figure 3 shows the dependence of average grain size on

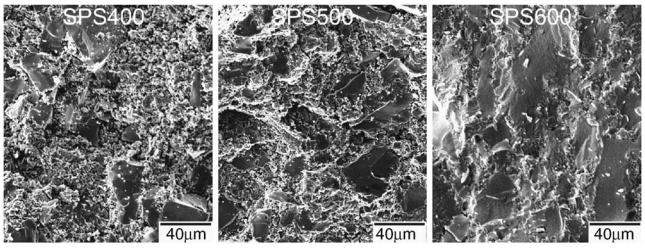

FIG. 1. SEM images of the SPS sintered samples.

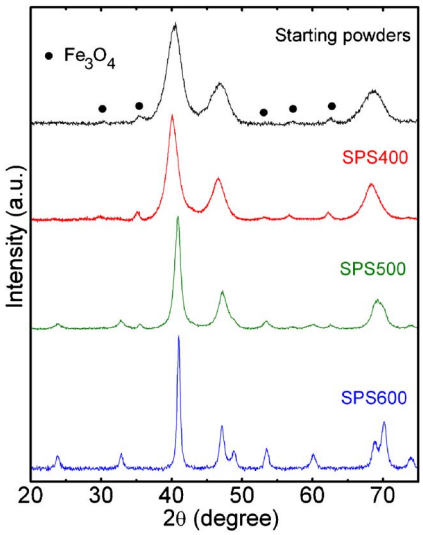

FIG. 2. XRD patterns of starting powders and SPS sintered samples.

the annealing temperature for the bulk sample sintered at different temperatures. The grain size was evaluated with XRD measurements using Williamson-Hall analysis for line broadening.[20] As one can see, the grain sizes are about 7.5 nm, 10.0 nm, and 17.3 nm for the SPS400, SPS500, and SPS600, respectively. The TEM analysis (as presented in Fig. 4) shows that the grain sizes are around 5–8 and 18–22 nm for SPS400 and SPS600, which agree with the XRD analysis. The selected area electron diffraction (SAED) patterns (not shown in the figure) confirmed the coexistence of fcc FePt and Fe_3O_4 phases in SPS400 and the disappearance of Fe_3O_4 phase in SPS600. As can be seen from Figs. 3 and 4, the grain sizes are quite small compared to those for materials fabricated by traditional techniques. It is also interesting to find that the grain size only increased to 23 nm for SPS600 sample even after annealing at 700 °C for 1 h.

The effort made in controlling grain size is to realize the effective intergrain magnetic exchange coupling. The δm measurements (Henkel plot)[21,22] were performed to compare the SPS nanocomposite magnets. It is found that the positive

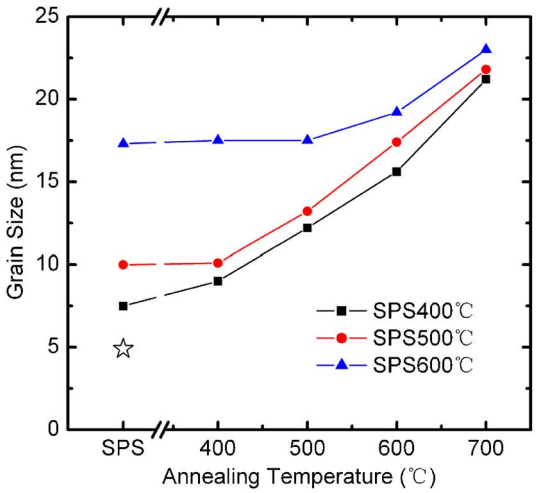

FIG. 3. The dependence of grain size on annealing temperature for SPS400, SPS500, and SPS600. The open star represents the grain size of the starting powders (4.9 nm).

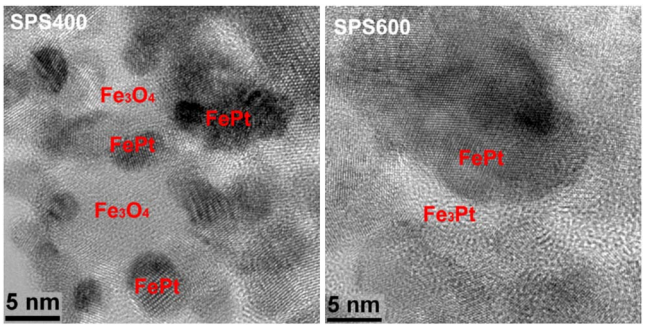

FIG. 4. TEM images of the as-sintered SPS400 and SPS600 bulks.

δm value, i.e., the exchange coupling, of the 400 °C annealed SPS600 sample is much higher than the 600 °C annealed SPS400+FG600. This means that pressure during the phase transition is more beneficial for the intergrain exchange coupling than that of a simple heating by annealing.

The magnetic properties of the SPS samples can be further improved by postannealing during which the formation of the $L1_0$ FePt phase and the Fe_3Pt phase was more complete. Figure 5 gives the dependence of magnetic properties on annealing temperature (T_a) of the SPS samples. It can be seen from Fig. 5 that the M_s of SPS400 and SPS500 increases with increasing T_a, which should be due to the decomposition of Fe_3O_4 phase and formation of Fe_3Pt phase as discussed above. While M_s of SPS600 almost fixed with varying T_a. This means that the Fe_3O_4 was almost decomposed during the sintering. This agrees with the oxygen content change. The as-sintered SPS400 shows zero coercivity H_c which means that the temperature of 400 °C is not high enough for phase transition from fcc to $L1_0$. The SPS500 shows a H_c around 1.5 kOe even the phase transition started since the chemical ordering S is only 0.58. The annealing

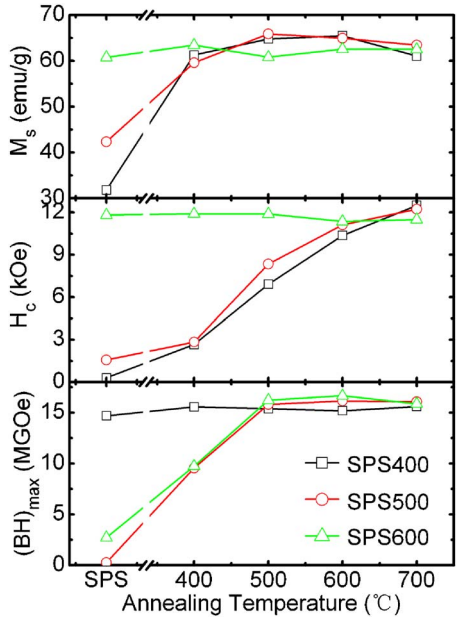

FIG. 5. The dependence of M_s, H_c, and $(BH)_{max}$ on annealing temperature under forming gas. The $(BH)_{max}$ values are calculated from full density. The annealing time is 1 hour and the ambience is forming gas (93%Ar+7%H_2).

thus increases the coercivity with increasing T_a for SPS400 and SPS500. However, for SPS600, S and H_c are fixed at around 0.8 and 11.5 kOe with varying T_a. With both high M_s and H_c, and strong intergrain exchange coupling, maximum energy products of 8.3 MG Oe calculated from real density and 16.5 MG Oe calculated from the full density can be obtained for SPS500 by annealing at 500–600 °C for 1 h.

In summary, FePt/Fe_3Pt bulk nanocomposite magnets have been obtained by the spark plasma sintering of chemically synthesized FePt and Fe_3O_4 nanoparticles. Density about 70% theoretical value has been obtained by the SPS technique. It is found that the phase transition from fcc to $L1_0$ structure starts at 500 °C and is almost completed at 600 °C. The density increases significantly during the phase transition, while the grain size is still retained in the nanoscale even after annealing at 700 °C. It is interesting to find that pressure during the phase transition is more beneficial for intergrain exchange coupling than that of simply sintering by annealing.

This work was supported by US DoD/MURI Grant No. N00014-05-1-0497 and DARPA through ARO under Grant No. DAAD 19-03-1-0038. The work at Ames Laboratory was supported by the United States Department of Energy (USDOE), Office of Science (OS), Office of Basic Energy Sciences (BES) through Iowa State University under Contract W-7405-ENG-82.

[1] R. Skomski and J. M. D. Coey, Phys. Rev. B **48**, 15812 (1993).
[2] C. B. Rong, H. W. Zhang, R. J. Chen, S. L. He, and B. G. Shen, J. Magn. Magn. Mater. **302**, 126 (2006).
[3] R. Fischer, T. Schrefl, H. Kronmuller, and J. Fidler, J. Magn. Magn. Mater. **150**, 329 (1995).
[4] C. B. Rong, H. W. Zhang, X. B. Du, J. Zhang, S. Y. Zhang, and B. G. Shen, J. Appl. Phys. **96**, 3921 (2004).
[5] E. Kneller and R. Hawig, IEEE Trans. Magn. **27**, 3588 (1991).
[6] Z. J. Guo, J. S. Jiang, J. E. Pearson, S. D. Bader, and J. P. Liu, Appl. Phys. Lett. **81**, 2029 (2002).
[7] Z. S. Shan, J. P. Liu, V. M. Chakka, H. Zeng, and J. S. Jiang, IEEE Trans. Magn. **38**, 2907 (2002).
[8] C. B. Rong, H. W. Zhang, X. B. Du, J. Zhang, S. Y. Zhang, and B. G. Shen, J. Magn. Magn. Mater. **277**, 221 (2004).
[9] H. Zeng, J. Li, J. P. Liu, Z. L. Wang, and S. H. Sun, Nature (London) **420**, 395 (2002).
[10] Z. G. Liu, M. Umemoto, S. Hirosawa, and H. Kanekiyo, J. Mater. Res. **14**, 2540 (1998).
[11] M. Yue, J. X. Zhang, Y. F. Xiao, G. P. Wang, and T. Li, IEEE Trans. Magn. **39**, 3551 (2003).
[12] T. Saito, J. Appl. Phys. **99**, 08B522 (2006).
[13] S. H. Sun, C. B. Murray, D. Weller, L. Folks, and A. Moser, Science **287**, 1989 (2000).
[14] S. H. Sun, H. Zeng, D. B. Robinson, S. Raoux, P. M. Rice, S. X. Wang, and G. X. Li, J. Am. Chem. Soc. **126**, 273 (2004).
[15] B. E. Warren, *X-Ray Diffraction* (Dover, New York, 1990), Chap. 12.
[16] S. H. Whang, Q. Feng, and Y. Q. Gao, Acta Mater. **46**, 6485 (1998).
[17] J. Lyubina, I. Opahle, K. H. Muller, O. Gutfleisch, M. Richter, M. Wolf, and L. Schultz, J. Phys.: Condens. Matter **17**, 4157 (2005).
[18] C. B. Rong, V. Nandwana, and N. Poudyal, Y. Li, J. P. Liu, Y. Ding, and Z. L. Wang, J. Phys. D **40**, 712 (2007).
[19] N. N. Greenwood and A. Earnshaw, *Chemistry of the Elements* (Butterworth, Oxford, 1997).
[20] K. Williamson and W. H. Hall, Acta Metall. **1**, 22 (1953).
[21] K. O'Grady, M. EL-Hilo, and R. W. Chantrell, IEEE Trans. Magn. **29**, 2608 (1993).
[22] C. B. Rong, H. W. Zhang, B. G. Shen, and J. P. Liu, Appl. Phys. Lett. **88**, 042504 (2006).